Wave chaos in the nonequilibrium dynamics of the Gross-Pitaevskii equation

Iva Březinová,[1,*] Lee A. Collins,[2] Katharina Ludwig,[1] Barry I. Schneider,[3,4] and Joachim Burgdörfer[1]

[1]*Institute for Theoretical Physics, Vienna University of Technology, Wiedner Hauptstraße 8-10/136, A-1040 Vienna, Austria, EU*

[2]*Theoretical Division, Los Alamos National Laboratory, Los Alamos, New Mexico 87545, USA*

[3]*Physics Division, National Science Foundation, Arlington, Virginia 22230, USA*

[4]*Electron and Atomic Physics Division, National Institute of Standards and Technology, Gaithersburg, Maryland 20899, USA*

The Gross-Pitaevskii equation (GPE) plays an important role in the description of Bose-Einstein condensates (BECs) at the mean-field level. The GPE belongs to the class of nonlinear Schrödinger equations which are known to feature dynamical instability and collapse for attractive nonlinear interactions. We show that the GPE with repulsive nonlinear interactions typical for BECs features chaotic wave dynamics. We find positive Lyapunov exponents for BECs expanding in periodic and aperiodic smooth external potentials, as well as disorder potentials. Our analysis demonstrates that wave chaos characterized by the exponential divergence of nearby initial wave functions is to be distinguished from the notion of nonintegrability of nonlinear wave equations. We discuss the implications of these observations for the limits of applicability of the GPE, the problem of Anderson localization, and the properties of the underlying many-body dynamics.

I. INTRODUCTION

Following the experimental realization of Bose-Einstein condensates (BECs) in dilute ultracold gases, the Gross-Pitaevskii equation (GPE), has taken center stage to describe the equilibrium as well as nonequilibrium dynamics of the condensate at the mean-field level [1]. The replacement of the many-body wave function by the effective single-particle condensate wave function has proven to be a remarkably successful approximation for predicting a large variety of physical observables [2]. Among the observables are both ground-state properties and elementary excitations in inhomogeneous background potentials [2–9]. The GPE belongs to the class of nonlinear Schrödinger equations (NLSEs) which have a broad range of applications ranging from nonlinear optics to plasma physics and Bose-Einstein condensation [10]. Effects beyond the GPE have been observed in BECs, most notably in optical lattices with deep wells and small occupation numbers per site. In this regime, explicit many-body descriptions such as the Bose-Hubbard model are more suitable [11,12]. The nonequilibrium dynamics of BECs, specifically their expansion in disordered potentials, has recently received a lot of attention (see, e.g., Refs. [3–9,13–21] and references therein). One focus is on the observation of Anderson localization of a quantum gas. For weak disorder potentials $\langle V \rangle \ll \mu$, where $\langle V \rangle$ is the variance of the potential and μ is the chemical potential of the BEC, the GPE was assumed to be valid during the nonequilibrium expansion starting from the BEC released from the trap to the dilute localized state for which the linear one-particle Schrödinger limit is reached [15,17]. The consequences of the presence of the nonlinearity for the nonequilibrium dynamics in a disordered potential described by the GPE deserves a careful analysis. The NLSE with attractive interactions is known to feature dynamical instabilities leading to collapse of the wave packet [2]. Closely related, the GPE with repulsive pair

interaction in a strictly periodic potential features near the Brillouin zone boundary a dynamical (modulation) instability since the effective negative-mass dispersion translates into an effective attractive pair interaction (see, e.g., Refs. [22–26] and references therein). Discretized models resembling the Fermi-Pasta-Ulam-Tsingou[1] system of nonlinearly coupled oscillators have been found to feature stochastic dynamics and relaxation with an increasing entropy [29–31].

We show in the following that the GPE for realistic parameters for the expansion of BECs in the quasi-one-dimensional (quasi-1D) regime displays true wave chaos as measured by a positive Lyapunov exponent in Hilbert space. By careful checks of the accuracy of the propagation including the method of time-reversed propagation, this "physical" chaos can be distinguished from the numerical chaos previously observed for the NLSE [29,32]. We furthermore show that chaos goes beyond the nonintegrability of nonlinear wave equations. The physical consequences of deterministic chaos in the GPE for smooth periodic and aperiodic potentials as well as disorder potentials will be discussed. We argue that wave chaos in the GPE is a signature for the breakdown of mean-field theory and delimits the border of its applicability. The latter does not preclude that certain ensemble expectation values of a BEC can be approximately accounted for by a GPE. We conjecture that the chaotic fluctuations are a signature of excitations and depletion of the condensate. Although our physical interpretations focus on BECs, our findings are relevant for other areas of application of the NLSE as well [33].

The paper is organized as follows. In Sec. II we briefly describe the model for the expansion of a quasi-1D BEC within the GPE. Numerical methods for the propagation of the condensate wave functions are reviewed in Sec. III.

---

*iva.brezinova@tuwien.ac.at

---

[1]The model is in literature known under the name Fermi-Pasta-Ulam [27]. We follow here the suggestion by T. Dauxois [28] to recognize the important contribution of M. Tsingou to this pioneering computational study.

Nonintegrability and wave chaos are discussed in Sec. IV, followed by numerical results in Sec. V. Conclusions and conjectures are given in Sec. VI.

II. GROSS-PITAEVSKII EQUATION FOR AN EXPANDING (QUASI)-1D BEC

The GPE for the inhomogeneous condensate wave function $\psi(\vec{r},t) = \langle \hat{\psi}(\vec{r},t) \rangle$, the nonvanishing expectation value of the field operator $\hat{\psi}(\vec{r},t)$ that becomes finite at the Bose-Einstein phase transition, is given by

$$i\hbar \frac{\partial \psi(\vec{r},t)}{\partial t} = \left(-\frac{\hbar^2 \nabla^2}{2m} + V(\vec{r}) + g_{3D} |\psi(\vec{r},t)|^2 \right) \psi(\vec{r},t). \tag{1}$$

The effective interparticle nonlinear coupling constant in three dimensions,

$$g_{3D} = \frac{4\pi \hbar^2 a_s}{m}, \tag{2}$$

is expected to account for the condensate dynamics under the conditions of low excitations, that is, weak depletion of the condensate, and of weak coupling. Moreover, Eq. (1) assumes short-range interactions at low energies such that the particle-particle interaction can be described by a contact interaction whose strength is proportional to the s-wave scattering length a_s. The mean-field approximation is assumed to be valid in the dilute regime $n^{1/3} a_s \ll 1$, where n is the particle density. We consider in the following a (quasi)-1D system, for example, a cigar-shaped trap where the radial and longitudinal frequencies are related as $\omega_r \gg \omega_l$ and we assume the chemical potential μ to be small compared to the transverse quantization energy $\mu \ll \hbar \omega_r$. Thus, the BEC is described by a 1D order parameter. In the transverse direction the dynamics is confined to the ground state. The 1D GPE is then given by

$$i\hbar \frac{\partial \psi(x,t)}{\partial t} = -\frac{\hbar^2}{2m} \frac{\partial^2}{\partial x^2} \psi(x,t) + V(x)\psi(x,t)$$
$$+ 2\hbar \omega_r a_s N |\psi(x,t)|^2 \psi(x,t). \tag{3}$$

The number of atoms N enters explicitly because we normalize the order parameter (in the following termed wave function) as $\int dx |\psi(x,t)|^2 = 1$. The potential $V(x)$ is an external potential to be described in more detail below. Measuring energies in units of the longitudinal oscillator energy $\hbar \omega_l$, length in units of the oscillator length $l_0 = (\hbar/m\omega_l)^{1/2}$, and time in units $t_0 = 1/\omega_l$, the GPE takes in these (oscillator) units the form

$$i \frac{\partial \psi(x,t)}{\partial t} = -\frac{1}{2} \frac{\partial^2 \psi(x,t)}{\partial x^2} + U(x)\psi(x,t)$$
$$+ g|\psi(x,t)|^2 \psi(x,t), \tag{4}$$

with $U(x) = V(xl_0)/\hbar \omega_l$, $g = 2(\omega_r/\omega_l)aN$, and $a = a_s/l_0$. In the following we refer to the effective Hamiltonian of the linear Schrödinger equation as $H_L = -\frac{1}{2} \frac{\partial^2}{\partial x^2} + U(x)$ and to the nonlinear part of the Hamiltonian as $H_{NL} = g|\psi|^2$.

Most of the numerical simulations presented in the following are performed for ultracold gases of Rb^{87} initially stored in a cigar-shaped trap with the following parameters: $N = 1.2 \times 10^4$ and $a_s = 5.82$ nm, and following Ref. [7] $\omega_l = 5.4 \times 2\pi$ Hz and $\omega_r = 70 \times 2\pi$ Hz. Accordingly, the unit of

time is $t_0 = 29.47$ ms and the unit of length is $l_0 = 4.64$ μm. The associated nonlinearity is

$$g_0 = 2\frac{\omega_r}{\omega_l}aN \approx 390 \tag{5}$$

for later reference. Note that the rather high numerical value for g_0 is due to the explicit inclusion of the number of particles N and does not contradict the assumption of weak coupling. For these parameters $\mu \ll \hbar \omega_r$ is not fulfilled, however, it is assumed that the BEC is in the quasi-1D regime such that a 1D order parameter is sufficient to describe the dynamics (see, e.g., Refs. [6,7,17,18] where the dynamics is essentially confined to its ground state in the transverse direction).

The GPE [Eq. (4)] can be derived as the Euler-Lagrange equation from a Lagrangian functional in the fields $\psi(x,t)$ and $\dot{\psi}(x,t)$. The corresponding Hamiltonian functional is given by

$$H[\psi] = \int dx \left(\frac{1}{2} |\partial_x \psi|^2 + U|\psi|^2 + \frac{g}{2} |\psi|^4 \right). \tag{6}$$

The total energy functional $E = H[\psi]$ must be conserved during the expansion of the BEC. This conservation law provides a stringent test for numerical stability of the long-time propagation.

III. NUMERICAL METHODS

The propagation of an initial condensate wave function $\psi(x,t=0)$ according to the GPE [Eq. (4)] proceeds by discretization of space and time. The space discretization must be performed carefully since simple discretization schemes may unintentionally convert the integrable continuous GPE into a discrete nonlinear system that displays chaos. For example, using the simplest finite difference scheme with $\delta x = x_{i+1} - x_i$, Eq. (4) with $U = 0$, takes the form

$$i\partial_t \psi_i = -\frac{1}{2\delta x^2}(\psi_{i+1} - 2\psi_i + \psi_{i-1}) + g|\psi_i|^2 \psi_i. \tag{7}$$

Equation (7) shows chaos [29] and has been used to study stochastic dynamics and thermalization in the mean-field Bose-Hubbard system [31] while its continuous limit is known to be integrable [29]. Since we want to study the continuous system we have to avoid such discretization artifacts by employing a more elaborate discretization. Our spatial discretization is based on the finite-element discrete variable representation (FEDVR) (see Refs. [34–37] and references therein). We split the space into finite elements which are discretized with the help of a discrete variable representation (DVR) basis. The basis consists of Lagrange interpolating polynomials determined via a grid consisting of the zeros of Legendre polynomials and the end points of each element. The elements are connected via bridge functions, thus guaranteeing the continuity of the wave functions. Integrals are approximated via the Gauss-Lobatto quadrature. In the FEDVR the local operators (e.g., the potential operators) are diagonal. The kinetic operator within a single element is a full $N_b \times N_b$ matrix when N_b is the number of basis functions. Within the FEDVR the Hamiltonian is a sparse matrix when the number of elements and basis functions are chosen appropriately.

For temporal propagation we tested several different propagators: the second-order difference [38,39] (SOD), the Runge-Kutta [40], the real space product split operator [39,41] (equivalent to the symplectic operator [42] SABA$_1$), the Crank-Nicholson [38], and the Lanczos propagators [39,43]. The Runge-Kutta and SOD algorithms have proven to be most accurate in terms of energy conservation. In most of our calculations we use the SOD algorithm. It is an explicit conditionally stable integration scheme given by the recursion relation

$$\psi(x, t + dt) = \psi(x, t - dt) - i2dt\hat{H}\psi(x, t), \quad (8)$$

where $\hat{H}$ is given by

$$\hat{H} = -\frac{1}{2}\frac{\partial^2}{\partial x^2} + U(x) + g|\psi(x, t)|^2. \quad (9)$$

The numerically more expensive fourth-order Runge-Kutta algorithm is used for cross-checking. Comparison with a fifth-order Runge-Kutta algorithm allows an accuracy estimate in $|\psi|^2$ to be of the order of 10^{-15} for each time step.

Both SOD and Runge-Kutta are not symplectic. The Hamiltonian structure of the GPE would suggest to use a symplectic integrator. Such integrators preserve, by design, the volume in phase space which is characteristic for the dynamics of Hamiltonian systems. However, it has been demonstrated for the NLSE and the Korteweg-deVries equation and conjectured for infinite dimensional Hamiltonian systems in general that the use of symplectic time integrators is less important than high accuracy of spatial derivatives [44,45]. For the results presented in the following we use the time increment $dt = 4 \times 10^{-6}$ and five basis functions for finite-element widths of typically $dx = 0.08$ in a box of size $x \in [-1000, 1000]$. (For the long time propagations presented in Sec. V C the box size is $x \in [-1600, 1600]$.) We use hard-wall boundary conditions for our numerical box. The numerical box is chosen sufficiently large such that the spreading wave packet $\psi(x, t)$ does not effectively reach the walls of the box within the time of propagation.

Apart from energy conservation, an additional sensitive test of the numerical stability of the propagation algorithm is the time reversal of propagation. Expressing the propagation of the initial condensate wave function $\psi(x, 0)$ as

$$\psi(x, t) = U_t[\psi(x, 0)], \quad (10)$$

the time-reversed propagation

$$\psi(x, 0) = U_{-t}[\psi(x, t)] \quad (11)$$

should recover the initial state. For the linear Schrödinger equation (LSE), reaching the initial state via Eq. (11) is easier than for the NLSE due to the intrinsic stability of the linear dynamical evolution. For the NLSE, Eq. (11) provides a measure for the accumulation of numerical noise, that is, a measure for "numerical chaos." [32]. In order to distinguish true deterministic ("physical") chaos from numerical noise, we probe the accuracy of Eq. (11) by quantifying how close the backward-propagated wave function will be to the initial state $\psi(x, 0)$.

Another stringent test results from the scaling property of the GPE. We subject the space and time coordinates to the scaling ($\gamma > 0$):

$$\begin{aligned} t &\to \bar{t} = t/\gamma, \\ x &\to \bar{x} = x/\sqrt{\gamma}. \end{aligned} \quad (12)$$

The GPE becomes, after multiplication by γ,

$$\begin{aligned} i\frac{\partial}{\partial \bar{t}}\psi(\bar{x}, \bar{t}) = &-\frac{1}{2}\frac{\partial^2}{\partial \bar{x}^2}\psi(\bar{x}, \bar{t}) + \bar{U}(\bar{x})\psi(\bar{x}, \bar{t}) \\ &+ \gamma g|\psi(\bar{x}, \bar{t})|^2\psi(\bar{x}, \bar{t}), \end{aligned} \quad (13)$$

with $\bar{U}(\bar{x}) = \gamma U(\sqrt{\gamma}x)$. The normalization of the condensate wave function after rescaling

$$\bar{\psi}(\bar{x}, \bar{t}) = \gamma^{1/4}\psi(\bar{x}, \bar{t}) \quad (14)$$

leads to the rescaled GPE:

$$\begin{aligned} i\frac{\partial}{\partial \bar{t}}\bar{\psi}(\bar{x}, \bar{t}) = &-\frac{1}{2}\frac{\partial^2}{\partial \bar{x}^2}\bar{\psi}(\bar{x}, \bar{t}) + \bar{U}(\bar{x})\bar{\psi}(\bar{x}, \bar{t}) \\ &+ \bar{g}(\gamma)|\bar{\psi}(\bar{x}, \bar{t})|^2\bar{\psi}(\bar{x}, \bar{t}), \end{aligned} \quad (15)$$

with $\bar{g}(\gamma) = \sqrt{\gamma}g$. Converged numerical solutions that are not subject to numerical noise will satisfy the scaling behavior [Eq. (15)] for every positive value of γ. Scaling is equivalent to a continuous variation of the spatiotemporal grid. One further consequence of Eq. (15) is that scaling corresponds to free tuning of the nonlinearity in the absence of $\bar{U}$. Therefore, thresholds for critical strength of nonlinearity, if they exist at all, can occur only in the presence of external potentials.

IV. INTEGRABILITY, NONINTEGRABILITY, AND WAVE CHAOS IN THE GPE

For nonlinear wave equations, the GPE being an example of which, integrability is closely associated with the existence of solutions via the inverse scattering transform (IST). Briefly, the initial value problem (IVP) of the nonlinear wave equation possesses an integrable solution if the solution can be determined by IST. In such a case, the nonlinear wave equation is associated with a system of auxiliary linear ordinary differential equations (LODEs) for which $\psi(x, t)$ acts as a "potential" and whose direct and inverse scattering solution solves the original IVP (see, e.g., Refs. [46–48]). The time t acts here as a "deformation parameter." While this criterion for integrability is explicit and constructive, it does not, however, provide *a priori* a sufficient criterion for nonintegrability.

For the GPE, a few special cases are known: For vanishing external potential, $U(x) = 0$, and infinite domain ($-\infty < x < \infty$), the GPE is integrable and the corresponding LODEs are the Zakharov-Shabat (ZS) system [46–48]. While for attractive interparticle interactions ($g < 0$), the ZS system features both a continuum and bound states corresponding to soliton solutions of the GPE, for repulsive interactions ($g > 0$), the case of interest in the following, the ZS spectrum is purely continuous corresponding to a dispersing (decaying) condensate wave function $\psi(x, t)$. For hard-wall Dirichlet boundary conditions, the GPE with $U(x) = 0$ was conjectured to be nonintegrable. [30].

For nonvanishing external potentials [$U(x) \neq 0$], no general results on the existence of integrable solutions of the GPE are known. For a few special cases, integrability has been demonstrated. These cases include the harmonic potential, $U(x) \propto x^2$, with time-dependent nonlinearities [49–51], and linear potentials, $U(x) \propto x$, with time-independent nonlinearity [52,53].

One test for integrability is the Weiss-Tabor-Carnevale (WTC) test for nonautonomous NLSEs with time- and space-dependent dispersion, nonlinearity, and dissipation [47]. The WTC test is based on the Painlevé conjecture (see, e.g., Refs. [47,48]) and provides a necessary condition for integrability (see Ref. [54] for specific potentials and nonlinearities). Another integrability condition is based on the Lax pair method yielding, in general, different criteria [55]. However, both integrability conditions agree in that for constant dispersion and nonlinearity and vanishing dissipation the potential $U(x)$ may be at most linear in x. For disordered potentials in the NLSE it was shown that quasiperiodic motion may persist for weak nonlinearities that can be considered as a small perturbation [56].

In the following we consider potentials $U(x)$ of physical interest which do not satisfy the known criteria of integrability. They include disordered, periodic, and aperiodic potentials. We characterize the resulting properties of the GPE by a stronger criterion than nonintegrability, that is, the appearance of wave chaos. As a measure for wave chaos we employ the existence of a positive Lyapunov exponent which indicates exponential sensitivity to initial conditions. In analogy to classical (particle) chaos, where the distance of initially close trajectories is followed in phase space, we follow the distance of initially close wave functions in Hilbert space. The metric in Hilbert space is the L^2 norm. Accordingly, we use a distance function:

$$d^{(2)}(\psi_1, \psi_2; t) = \frac{1}{2} \langle \psi_1 - \psi_2 | \psi_1 - \psi_2 \rangle$$
$$= \frac{1}{2} \int_{-\infty}^{\infty} dx \, |\psi_1(x,t) - \psi_2(x,t)|^2. \quad (16)$$

The Lyapunov exponent follows as the limit

$$\lambda = \frac{1}{2} \lim_{t \to \infty} \lim_{d^{(2)}(\psi_1,\psi_2;0) \to 0} \ln \frac{d^{(2)}(\psi_1,\psi_2;t)}{d^{(2)}(\psi_1,\psi_2;0)}. \quad (17)$$

In analogy to chaos for point particles, λ is only well-defined in terms of a coupled double limit. The distance function $d^{(2)}$ [Eq. (16)] for normalized functions and norm-conserving evolution reduces to

$$d^{(2)}(\psi_1, \psi_2) = 1 - \text{Re}\langle \psi_1 | \psi_2 \rangle. \quad (18)$$

It is bounded by $0 \leqslant d^{(2)} \leqslant 2$. The upper bound corresponds to $\psi_1 = -\psi_2$. The value 1 is reached for complete orthogonality and thus corresponds to the "maximal" separation in Hilbert space. Therefore, we expect that an exponential separation of initially "nearby," that is, almost identical, wave functions will eventually saturate at values $d^{(2)} \approx 1$. Equation (17) can be viewed as a measure for the exponential separation of trajectories in Hilbert space on the hypersphere S of unit radius defined by wave functions of unit norm. In practice, λ is numerically determined by the slope of that segment of growth on a semi-log plot that is approximately linear. The choice

of initial displacements $d^{(2)}(\psi_1, \psi_2; t)$ admitted in Eq. (16) is constrained by the Hamiltonian structure of the GPE with its corresponding energy shells, that is, $H[\psi_1] = H[\psi_2] = E$. With this constraint, the evolution of ψ_1, ψ_2 proceeds on a hypersphere in Hilbert space of fixed E.

It is instructive to first explore the short-time behavior of $d^{(2)}(\psi_1, \psi_2; t)$. The point of reference is the LSE, for which $d^{(2)}$ is strictly conserved, $d^{(2)}(\psi_1, \psi_2; t) = d^{(2)}(\psi_1, \psi_2; 0)$. Variation of $d^{(2)}$ is therefore a direct measure for the influence of the nonlinearity. For the nonlinear GPE, we obtain for initial real wave functions $\psi_1(x,0)$ and $\psi_2(x,0)$ up to second order in t

$$\text{Re}\langle \psi_1(t) | \psi_2(t) \rangle = c_0 + c_2 t^2 + O(t^4), \quad (19)$$

with

$$c_0 = \langle \psi_1(0) | \psi_2(0) \rangle = 1 - d^{(2)}(\psi_1, \psi_2; 0) \quad (20)$$

and

$$c_2 = \frac{g}{2} \int dx \, \psi_1(x,0)[n_1(x,0) - n_2(x,0), H_L]\psi_2(x,0)$$
$$- \frac{g^2}{2} \int dx \, \psi_1(x,0)[n_1(x,0) - n_2(x,0)]^2 \psi_2(x,0), \quad (21)$$

with $n_i(x,0) = |\psi_i(x,0)|^2$ the condensate density. The square bracket in the first term of Eq. (21) denotes the usual quantum mechanical commutator. For strongly interacting condensates where the interaction energy is large compared to the single-particle energies, the g^2 term in Eq. (21) dominates. The initial quadratic increase of the distance function $d^{(2)}$ with time is universal and independent of integrability, nonintegrability, or wave chaos. The short-time behavior of the distance function for a freely expanding condensate [$U(x) = 0$] released from a harmonic trap displays the growth with t^2 followed by saturation (Fig. 1). We conjecture that this saturation is a signature of the integrability of the GPE for $U(x) = 0$.
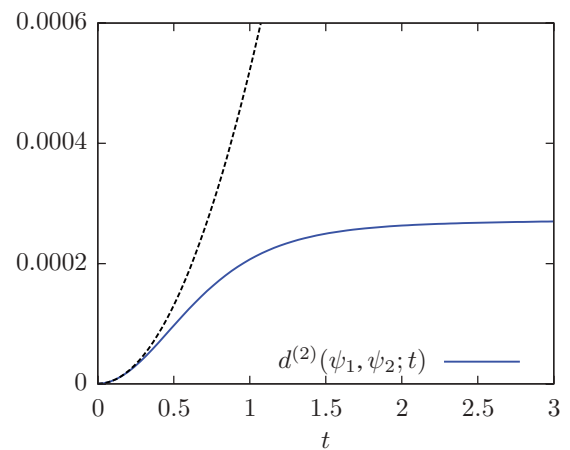

FIG. 1. (Color online) Distance function $d^{(2)}(\psi_1, \psi_2; t)$ [Eq. (16)] for a freely expanding BEC [$U(x) = 0$] with nonlinearity g_0 released from a harmonic trap (blue solid line). The initial normalized states ψ_1, ψ_2 are slightly perturbed ground states of the interacting system in the harmonic trap with a small linear perturbation [same states as will be used and explained in more detail in Eq. (23) in Sec. V]. The initial distance function is $d^{(2)}(0) \approx 2.8 \times 10^{-7}$. The black dashed line corresponds to $d^{(2)}(\psi_1, \psi_2; t)$ according to Eqs. (18) and (19).

A slightly different problem, expansion of a condensate in zero potential [$U(x) = 0$] inside a box defined by Dirichlet boundary conditions, was investigated by Villain and Lewenstein [30]. Motivated by the structural similarity to the famous Fermi-Pasta-Ulam-Tsingou model, they observed stochastic behavior as extracted from a normalized statistical entropy. For sufficiently strong nonlinearity a trend toward equipartition of energy among the modes of the LSE was found. The authors identified the free GPE with Dirichlet boundary conditions as nonintegrable. We have investigated the behavior of the distance function $d^{(2)}$ for this system. We follow Ref. [30] and choose as an initial state a Gaussian wave packet $\psi_G(x)$ with width $\sigma = 1$ in a box of length $L = 20$. This initial state is slightly distorted by a small linear admixture of strength α,

$$\psi_{1,2}(x,0) = N_{1,2}(1 \pm \alpha x)\psi_G(x), \qquad (22)$$

with normalization constants $N_{1,2}$. We test the sensitivity of $d^{(2)}(t)$ to α [i.e., to $d^{(2)}(0)$] by choosing two different values for α: $\alpha = 5 \times 10^{-4}$, which gives a similar initial $d^{(2)}(0)$ as in Fig. 1, and $\alpha = 5 \times 10^{-5}$, for which $d^{(2)}(0)$ is two orders of magnitude smaller. The numerical results confirm the expectation that $d^{(2)}(t)$ is linearly proportional to the initial distance $d^{(2)}(0)$ (constant shift in a logarithmic plot; see Fig. 2). For the strength of the nonlinearity we consider both a moderately strong value $g/L \approx 79\epsilon_1$, where $\epsilon_1 = \pi^2/2L^2$ is the ground-state energy of the LSE in the box comparable to the value ($g/L \approx 61\epsilon_1$) in Ref. [30], and a much stronger nonlinearity ($g/L \approx 1582\epsilon_1$), corresponding to g_0 [Eq. (5)]. The energy unit in Ref. [30] is related to our energy unit as $\epsilon_1 = 0.0123\hbar\omega_l$. The time unit $T_1 = 4L^2/\pi \approx 500t_0$ is long compared to our "oscillation" time scale t_0 characterizing the initial state.

For both nonlinearities the distance function $d^{(2)}(t)$ increases quadratically with a slope approximately proportional to the nonlinearity (see Fig. 2), in qualitative accord with the short-time behavior [Eqs. (18) and (19)], however with much reduced slope. The growth seen in Fig. 2 proceeds slowly. The quadratic increase is fundamentally different from the exponential increase observed in the following sections. This allows identifying within nonintegrable systems those that do not exhibit wave chaos, as in Ref. [30], and those that do, as the systems discussed in the following.

The overall quadratic rise is modulated by fluctuations which result from partial revivals of the underlying LSE (see inset of Fig. 2). One prominent oscillation period is $T_1/8$ corresponding to the inverse energy spacing between the two lowest LSE states of even parity [30]. Another prominent period $T_1/4$ results from the classical periodic orbit in the box. The nonlinearity leads to a proliferation of frequencies by side-band coupling.

The important conclusion is that the nonintegrable dynamics of the free GPE in a box with hard walls is, despite its complex appearance and the trend toward equipartition among the linear modes, nonchaotic as measured by the exponential separation of nearby trajectories in Hilbert space. Chaos requires the presence of nonvanishing external potentials $U(x)$.
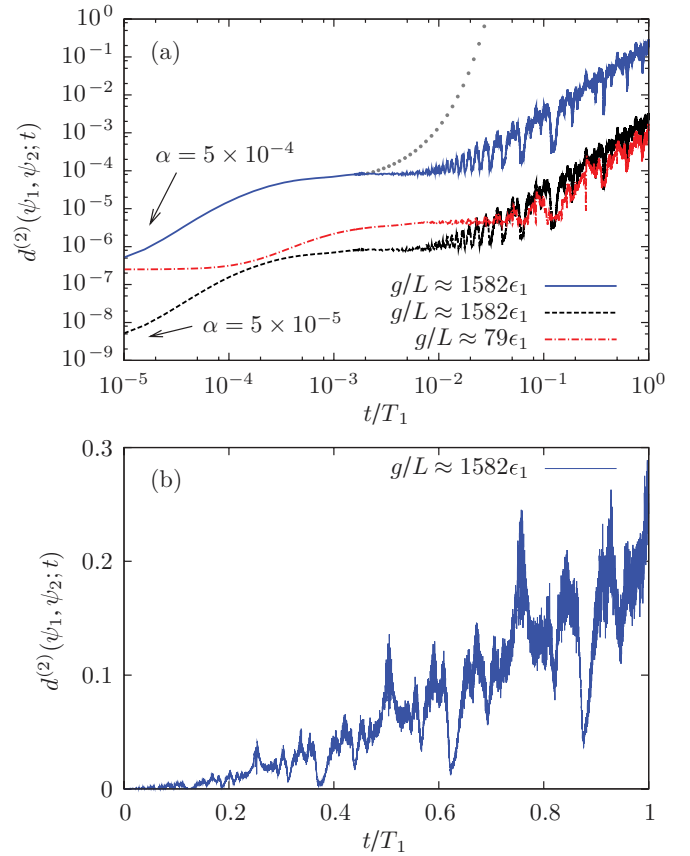

FIG. 2. (Color online) (a) Log-log plot of the distance function $d^{(2)}(\psi_1, \psi_2; t)$ [Eq. (16)] as a function of t for two initially nearby Gaussian wave packets in the box of length L obtained from propagation of the GPE with moderate nonlinearity ($g/L \approx 79\epsilon_1$) and strong nonlinearity ($g/L \approx 1582\epsilon_1$). For $g/L \approx 1582\epsilon_1$ two different distortion parameters α [see Eq. (22)] were used, $\alpha = 5 \times 10^{-4}$ and $\alpha = 5 \times 10^{-5}$ (marked by arrows in the figure). Time is measured in units of $T_1 = 2\pi/\epsilon_1$. For reference, the exponential growth in case of wave chaos with a Lyapunov exponent as in Fig. 4 is shown as a dotted line. (b) The curve with $g/L \approx 1582\epsilon_1$ and $\alpha = 5 \times 10^{-4}$ in linear scale.

V. NUMERICAL EXAMPLES FOR WAVE CHAOS

We present in this section examples for expansion of BECs in potentials $U(x)$ of experimental relevance. For the generation of nearby initial states we use the following scenario: The BEC is created in a harmonic trap; that is, the condensate wave function is given by the ground state of the GPE, $\psi_g(x)$, which is close to the Thomas-Fermi profile for the parameters chosen (see Sec. II). Two nearby normalized states are then created by weak perturbations linear in x,

$$\psi_{1,2}(x,0) = N_{1,2}(1 \pm \alpha x)\psi_g(x), \qquad (23)$$

with normalization constants $N_{1,2}$. Simultaneously with the release at $t = 0$ the external potential $U(x)$ is switched on. For the perturbation parameter α controlling the distance between ψ_1 and ψ_2 we typically choose $\alpha = 10^{-4}$. We have verified that the extracted values for the Lyapunov exponent λ are independent of the value of α.

A. Weak periodic potential

We first consider the expansion of the BEC in weak periodic potentials,

$$U(x) = U_0 \cos\left(2\pi x/l\right), \tag{24}$$

with periodicity l and strength of the weak potential U_0. We require

$$U_0/\epsilon \ll 1, \tag{25}$$

where $\epsilon = E/N$ is the total energy per particle of the interacting system. We use in the following $U_0 = 0.2\epsilon$. The chemical potential is to a good degree of accuracy $\mu(t = 0) = 2\epsilon$ at $t = 0$ for our choice of initial conditions. Unlike ϵ, $\mu(t)$ is not conserved during the expansion and, therefore, we use ϵ as characteristic energy scale. The periodic potential gives rise to a band structure of the linear problem with bandwidth of the first band, $W = \pi^2/2l^2$ (in literature also called recoil energy [26]), and a band gap at the first Brillouin zone boundary, $\Delta \approx U_0$. The wide band-gap limit corresponds to $W/U_0 \ll 1$, the nearly free particle limit to $W/U_0 \gg 1$. The spatial periodicity l is assumed to exceed the coherence (healing) length ξ of the condensate

$$l \gtrsim \xi, \tag{26}$$

with

$$\xi = \frac{1}{\sqrt{8\epsilon}}. \tag{27}$$

In the opposite limit $\xi \ll l$, the condensate can no longer resolve the local variation of the potential.

The initial wave functions are chosen as above [Eq. (23)] having identical energy in the potential [Eq. (24)] and a Thomas-Fermi length of $L_{\text{TF}} \approx 8.4$, which is larger than the potential periodicity $l = 5.8\xi$ with $\xi = 0.0945$. The nonlinearity is $g_0 \approx 390$. For $t > 0$ the condensate wave functions expand and acquire an increasingly complex fluctuation pattern. Appreciable deviations start to emerge near the center $x = 0$, where fluctuations have the largest amplitude [see Fig. 3(a)]. The deviations increase with increasing time [see Fig. 3(b)], such that locally the amplitudes of ψ_1 and ψ_2 become uncorrelated [see the inset of Fig. 3(b)]. Such an extreme sensitivity to initial conditions is the hallmark of wave chaos. It is worth noting that on the length scale of l both wave functions tend to mimic the oscillations of the potential while on larger length scales fluctuations of ψ_1 and ψ_2 lose their correlation.

We quantify the loss of correlation and the seemingly random fluctuations by the Lyapunov exponent λ [Eq. (17)]. Positive λ signifies wave chaos. The time evolution of the distance function $d^{(2)}(\psi_1, \psi_2; t)$ resembles the time evolution of particle chaos. After an initial generic nonexponential (quadratic) growth (see Fig. 4), $d^{(2)}$ grows exponentially until the regime of fluctuations around the saturation value is reached. The slope of the exponential growth makes it possible to numerically extract the Lyapunov exponent ($\lambda \approx 0.7$ for the case of Fig. 4).

The deterministic nature of the the exponential separation can be verified by the time-reversal test [Eq. (11)]. Upon
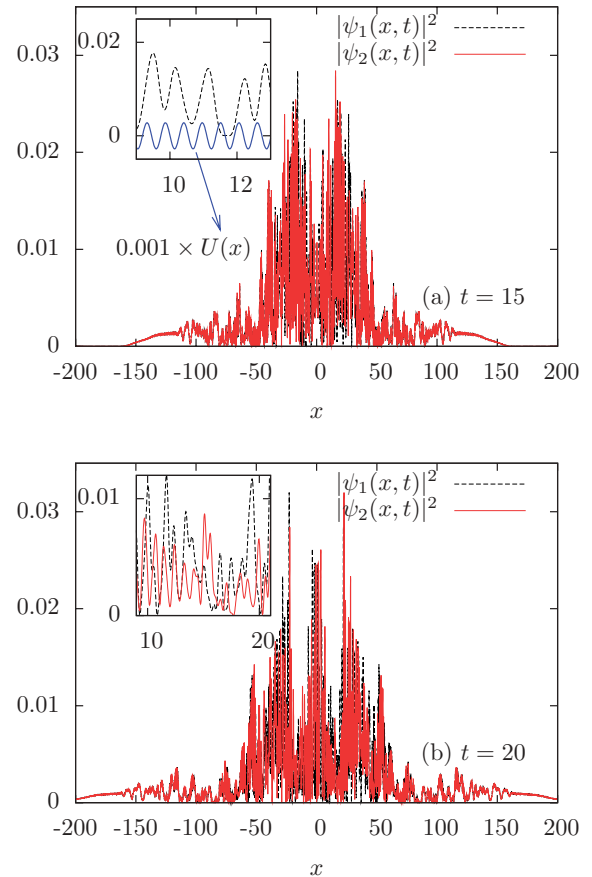

FIG. 3. (Color online) Onset of divergence between ψ_1 and ψ_2 as a function of time. $|\psi_1|^2$ and $|\psi_2|^2$ are given for (a) $t = 15$ and (b) $t = 20$. Inset in (a): comparison of the spatial fluctuations of the wave function and the period of the potential $U(x)$. The potential parameters are $U_0 = 0.2\epsilon$ and $l = 5.8\xi$. The nonlinearity is g_0. Inset in (b): increasingly uncorrelated fluctuations of $|\psi_1|^2$ and $|\psi_2|^2$.

reversal of the direction of time, the two condensate "trajectories" approach each other again to distances close to their
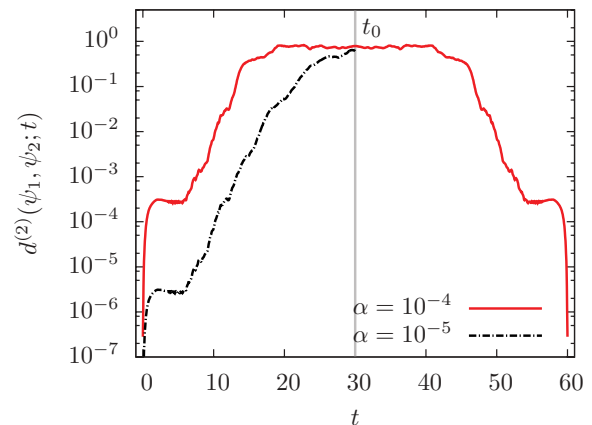

FIG. 4. (Color online) Exponential growth of $d^{(2)}$ for two condensate wave functions propagated by the GPE in a weak periodic potential (same parameters as in Fig. 3). Time-reversed propagation for $t > t_0$ recovers the initial state precluding numerical noise as origin of the exponential growth. Two different distortion parameters have been used: $\alpha = 10^{-4}$ and $\alpha = 10^{-5}$.
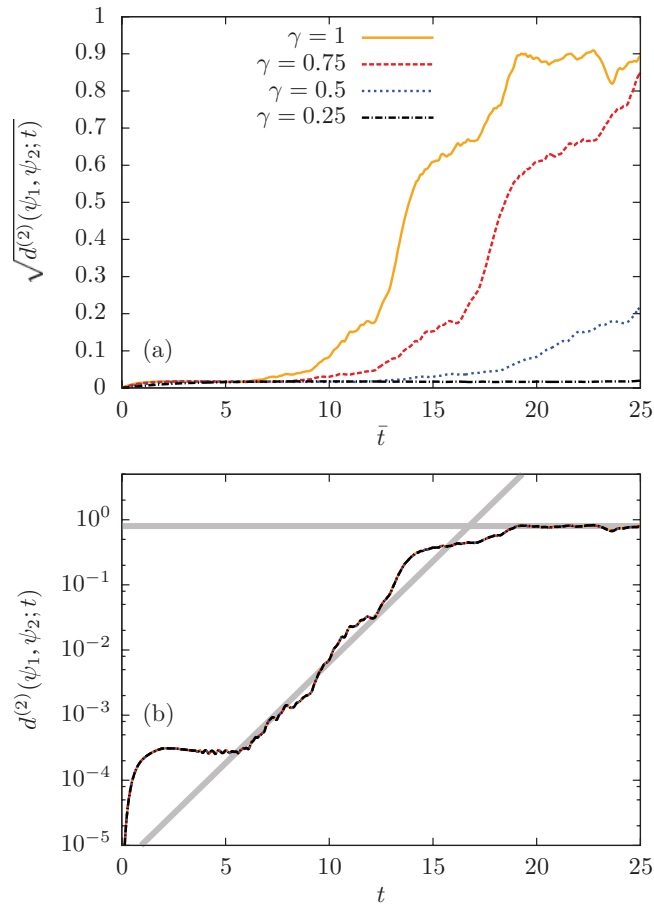
FIG. 5. (Color online) Distance $d^{(2)}$ between ψ_1 and ψ_2 as a function of time for different γ. The parameters of the periodic potential are $\bar{U} = 0.2\bar{\epsilon}$ and $\bar{l} = 5.8\bar{\xi}$. (b) Logarithmic plot of (a) squared after rescaling time according to $t = \gamma\bar{t}$. The curves coincide. The gray solid lines underline the region of exponential growth and saturation and are guides for the eye.

initial value (Fig. 5). The distance function between $\psi_1(x,0)$ and $U_{-t}[\psi_1(x,t)]$ is of the order of 10^{-9}. The near-perfect reversibility precludes numerical noise or "numerical chaos" as a source for divergence.

Furthermore, the scaling property of the GPE [Eq. (15)] is verified to a high degree of accuracy (Fig. 5). We scale the initial conditions according to $\bar{\mu}(t = 0) = \gamma\mu(t = 0)$, such that $\bar{U}/\bar{\epsilon}$ is constant. Likewise, the period of the potential is scaled such that $\bar{l}/\bar{\xi} = \sqrt{\gamma}l/\sqrt{\gamma}\xi$ is kept fixed. Despite a large absolute variation of $d^{(2)}$ with γ [Fig. 5(a)], upon rescaling, $d^{(2)}$ coalesces to a remarkable degree of accuracy [Fig. 5(b)]. The γ scaling is also equivalent to an effective change of the numerical grid in (x,t), that is, an increase of the numerical accuracy, since we have used the same absolute grid size for all calculations. The invariance of the results clearly demonstrates numerical stability. Since the Lyapunov exponent scales inversely with time $\bar{\lambda} = \gamma\lambda$, λ decreases with decreasing γ in accordance with Fig. 5(a). Note, however, that this power-law scaling does not provide information on the existence (or absence) of critical thresholds for wave chaos (see below).

In the single-band mean-field Bose-Hubbard model, a threshold for stochastic dynamics has recently been observed [31]. We explore now the behavior of λ in the continuum analog, the GPE with a periodic potential. The Lyapunov exponent λ will, in general, depend on the nonlinearity g, the period l, and the amplitude U_0 of the potential. The corresponding three energy scales are the total energy per particle ϵ (controlled by the nonlinearity g), the bandwidth of the first band W, and the amplitude U_0. The scaling property makes it possible to interrelate the dependences of λ on these three parameters. For example, one can investigate the dependence of λ on the ratio ϵ/W at constant U_0 by keeping ϵ constant and decreasing W (increasing l), giving the Lyapunov exponent $\lambda_{(\epsilon)}$, or keeping W constant and increasing g, hence, ϵ giving $\lambda_{(W)}$. If the ratio ϵ/W remains invariant for the two cases, the Lyapunov exponents are interrelated by the scaling property (provided one of the initial wave functions is rescaled) as $\lambda_{(\epsilon)} = \gamma\lambda_{(W)}$ with $\gamma < 1$. Therefore, it is sufficient to consider the ratio ϵ/W and not W and ϵ separately. We arrive at a two-dimensional parameter plane (U_0/ϵ, ϵ/W). A scan of λ is performed from the first to the second band of the linear system.

We observe a clear threshold of λ in form of a rapid increase along both the U_0/ϵ and the ϵ/W axis (see Fig. 6). Below the threshold λ is vanishing. A power-law fit to the threshold line gives $\epsilon/W \propto (U_0/\epsilon)^{-0.65}$ (see dashed line in Fig. 6). As the control parameter ϵ/W can be related to the parameter κ, the ratio between the nonlinearity parameter and the hopping parameter of the discrete system, it is suggestive to assume that the transition in the discrete system [31] and in the
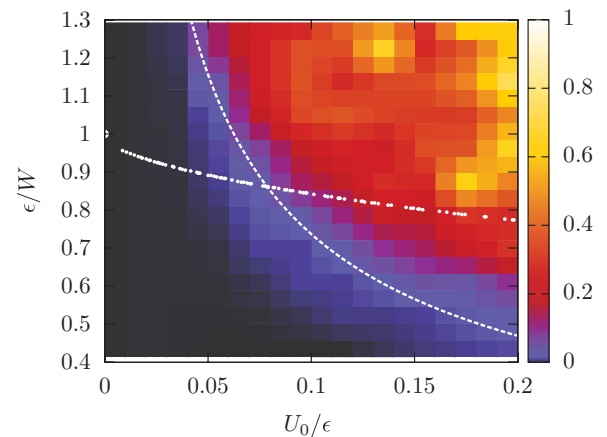

FIG. 6. (Color online) The Lyapunov exponent λ as a function of ϵ/W and U_0/ϵ. ϵ is the energy per particle, $W = \pi^2/2l^2$ is the bandwidth of the first band of the linear system, and U_0 is the amplitude of the potential [Eq. (24)]. The period l is kept fixed $l = 0.548\,11$. The same initial wave function has been used for all data points. λ has been determined numerically via a linear fit to the logarithmic increase of $d^{(2)}$ [Eq. (16)]. The deviation (summed absolute difference between the linear fit and the numerical curve) is on average well below 0.4 and maximal $\approx$0.6. To improve the graphical appearance, every second point in the figure is an interpolation between two numerical points. The white dashed curve is a fit to the threshold according to $\epsilon/W = 0.165(U_0/\epsilon)^{-0.65}$. The white dots mark the point where the energy ϵ equals the energy at the point of inflection of the first band.

present continuous system are of common origin. However, the discrete system does not account for the transition along U_0/ϵ. In other words, the mapping to the single-band Bose-Hubbard is not straightforward and a comparison to a multi-band model seems to be necessary.

Exponential divergence of wave functions above a threshold resembles the dynamical (or modulation) instability previously observed [22,24,26]. The modulation instability can be related to energetically surpassing the point of inflection along the first band of the linear problem: When the second derivative of the dispersion relation turns from positive to negative [24]. The position of the inflection point, however, does not agree with the position of the threshold (in Fig. 6 marked by white dots). The reason may be that the simplified picture of modulation instability also does not account for the threshold along U_0/ϵ. More importantly, the threshold does not seem to be sensitive to specific features of the linear problem, as presented in the next section.

B. Weak aperiodic potential

In order to explore whether wave chaos in the GPE is a specific feature of the interplay between the periodic linear problem and the nonlinearity, we investigate the dynamics in a strictly aperiodic potential,

$$U(x) = U_0[c_1 \cos(2\pi x/l_1) + c_2 \cos(2\pi x/l_2)], \quad (28)$$

where $l_2/l_1 = \frac{1}{2}(1 + \sqrt{5})$ is the "most" irrational golden mean number and $c_1 = c_2 = 1/2$. A well-defined band gap or well-defined negative mass dispersion relation near the Brillouin zone boundary which invoked the explanation of instability and stochastic motion [22,24,26] are absent for Eq. (28). For comparable values of U_0/ϵ as in the periodic case we find positive Lyapunov exponents (see Fig. 7). Interestingly, the threshold as well as the overall behavior agree well with the periodic case, suggesting that chaos does not depend on the specifics of the linear system but rather on the overall length and energy scales. In agreement with Fig. 6, the threshold shifts toward smaller values of U_0/ϵ for higher ratios of ϵ/W [Figs. 7(a) and 7(b)]. Note that a characteristic energy W can be defined for any potential with a characteristic length l_c as $W \propto 1/l_c^2$. Obviously, the wave chaos we have identified in the GPE is a general feature not coupled to specific properties of the band structure of the periodic linear problem.

C. Weak disorder

A further generalization is the GPE with random disorder replacing the smooth (a)periodic potential. This case is of particular interest in the context of Anderson localization recently studied for expanding BECs [7,8]. The latter experimental observations refer to the (quasi)linear regime when the nonlinearity was sufficiently weak such that the localization dynamics is governed by the Schrödinger equation. Localization in the presence of interactions has remained an open question. For the discrete NLSE, subdiffusive expansion rather than localization was observed numerically [20,57,58]. We focus on the interplay between the randomness induced by the potential and by the wave chaos in the GPE.
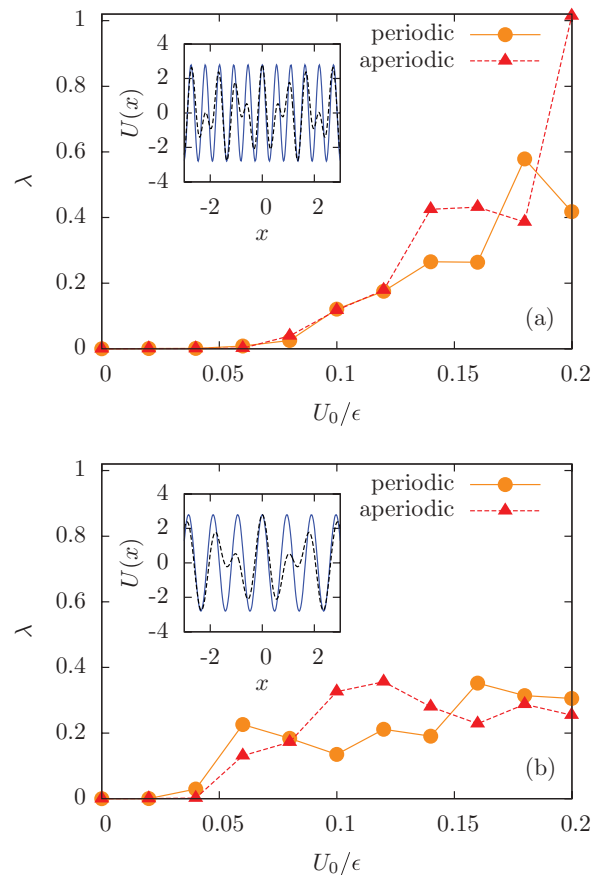

FIG. 7. (Color online) Lyapunov exponent λ as a function of U_0/ϵ for the periodic and aperiodic potentials. The period of the periodic potential is (a) $l = 0.548\,11$ and (b) $l = 0.945\,03$. l_1 of the aperiodic potential [Eq. (28)] is chosen respectively $l_1 = l$. The potentials are given in the inset. The energy $\epsilon \approx 14$ is constant such that ϵ/W is larger in (b) $\epsilon/W \approx 2.5$ than in (a) $\epsilon/W \approx 0.85$.

We follow closely the scenario employed in the investigations of Anderson localization [7,17]: The BEC initially trapped in a harmonic oscillator expands in a disorder potential. We construct a disorder potential with Gaussian correlation and zero mean. At N_d equidistant grid points x_i we place Gaussians with width σ and random weight A_i:

$$\tilde{U}(x) = \sum_{i=1}^{N_d} A_i e^{\frac{-(x-x_i)^2}{2\sigma^2}}. \quad (29)$$

After subtracting the mean, $\Delta U(x) = \tilde{U}(x) - \langle \tilde{U}(x) \rangle$, and normalizing by the standard deviation, $\langle \Delta U(x)^2 \rangle^{1/2}$, the disorder potential becomes (Fig. 8)

$$U_d(x) = \frac{U_0}{\langle \Delta U(x)^2 \rangle^{1/2}} \Delta U(x). \quad (30)$$

For U_0 we choose the same values as in the cases of periodic and aperiodic potentials above. The disorder potential Eq. (30) is by construction Gaussian correlated,

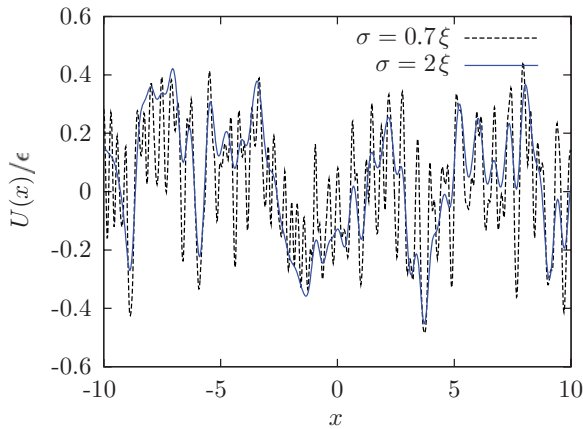$$C(x) = \langle U_d(x_0 + x) U_d(x_0) \rangle = U_0^2 e^{\frac{-x^2}{(2\sigma)^2}}, \quad (31)$$

FIG. 8. (Color online) Disorder potential for different values of the correlation length σ. The amplitude for both potentials is $U_0 = 0.2\epsilon$ and $N_d = 2 \times 10^4$. The energy ϵ and healing length ξ correspond to the ground state of the GPE in a harmonic oscillator at nonlinearity g_0 [Eq. (5)].

with a Gaussian-shaped Fourier transform (Fig. 9):

$$\tilde{C}(k) = \sqrt{2}\sigma U_0^2 e^{-k^2\sigma^2}. \tag{32}$$

Unlike for speckle potentials, the averages over odd powers $\langle U_d^{2n+1} \rangle$ vanish (numerically only approximately). The correlation length of the disorder potential σ provides a length scale competing with the healing length ξ of the free condensate.

For $\sigma < \xi$ the wave function is exponentially localized [17], which is characteristic for Anderson localization [see Fig. 10(b)]. For $\sigma > \xi$ (we have chosen $\sigma = 2\xi$), the condensate wave function develops algebraically decaying tails [17] that travel seemingly undisturbed through the disorder potential similar to propagation in free space [see Fig. 10(a)].

We probe for wave chaos for these two cases. It should be noted that in the presence of disorder, the determination of the exponential separation of nearby initial wave functions on the energy hypersphere faces the additional difficulty that it is not straightforward to create two nearby wave functions $\psi_1(x,0)$
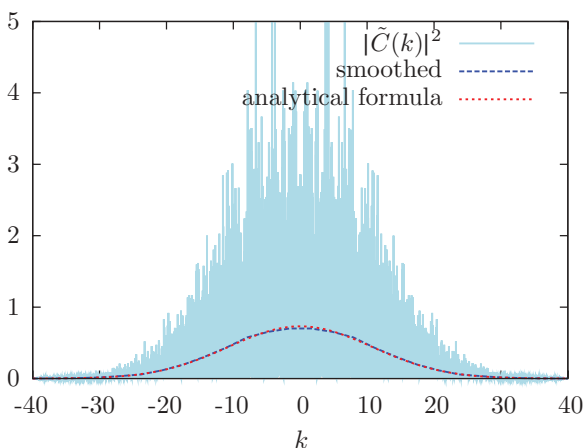

FIG. 9. (Color online) The Fourier transform of the correlation function $\tilde{C}(k)$ for $U_0 = 0.2\epsilon$ and $\sigma = 0.7\xi$ (Fig. 8). $\tilde{C}(k)$ agrees very well with Eq. (32) when smoothed over the fluctuations.
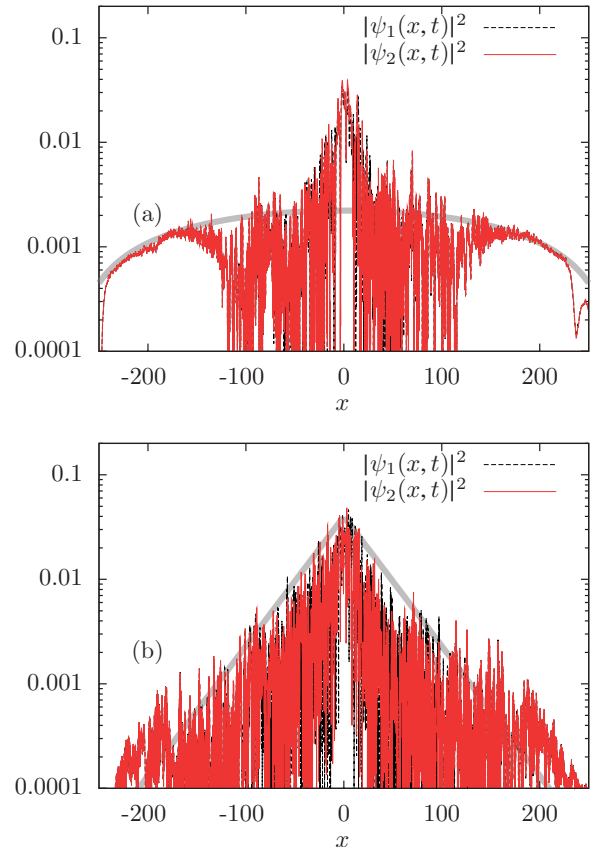

FIG. 10. (Color online) Chaotic fluctuations of ψ_1 and ψ_2 at $t = 24$ for (a) $\sigma = 2\xi$ in the algebraic regime and (b) for $\sigma = 0.7\xi$ in the "localized" regime (in the potentials of Fig. 8). The local fluctuations of ψ_1 and ψ_2 strongly deviate.

and $\psi_2(x,0)$ with equal energy. In the present case the energies of the wave functions are kept close with a relative deviation of the order of 10^{-4}.

In both cases, the algebraic and the exponential regime, we observe an exponentially growing separation and eventual saturation near the maximal value of separation $d^{(2)}(\psi_1,\psi_2) \approx 1$, confirming the intuitive notion that a random potential induces wave chaos. The Lyapunov exponent is $\lambda \approx 0.85$ in the algebraic regime [Fig. 10(a)] and $\lambda \approx 0.86$ in the exponential regime [Fig. 10(b)].

It is instructive to inquire into the relation between wave chaos and localization. Wave chaos is a signature of the nonlinearity in the wave equation, while localization is the hallmark of disorder in the linear wave equation. In discrete nonlinear models a variety of relations have been observed, one of which is subdiffusive growth rather than localization (see, e.g., Ref. [58] and references therein). As measure for the localization dynamics we use the time evolution of the variance of the condensate wave function, $\Delta x = \sqrt{\langle x^2 \rangle - \langle x \rangle^2}$. Note that our measure for the width is the square root of the second moment m_2 in Ref. [58]. We observe (Fig. 11) for the expansion in a disorder potential a slowing down of the spread which locally scales like $\Delta x \propto t^a$. In qualitative agreement with the prediction in Ref. [58] the exponent is not constant but changes over time. We observe for the system in Fig. 11 with nonlinearity g_0 an exponent of $a \approx 0.75$ up to $t = 60$ (compare our
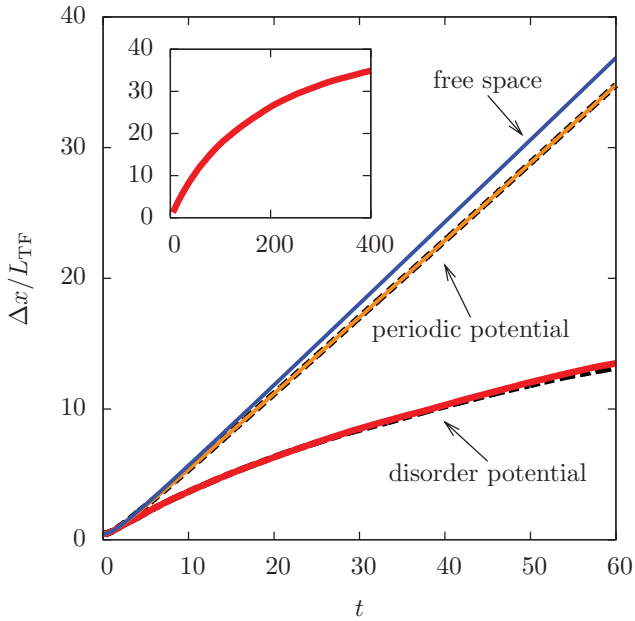
FIG. 11. (Color online) The variance Δx of the wave function $\psi_1(x,t)$ for propagations in free space, in a periodic potential ($U_0 = 0.2\epsilon$, $l = 20\xi$) and in a disorder potential ($U_0 = 0.2\epsilon$ and $\sigma = 0.7\xi$ as in Fig. 8). The black dashed lines correspond to $\psi_2(x,t)$ for the periodic and disorder potentials where chaos is present. The nonlinearity is $g_0 \approx 390$. The inset gives a long time evolution for a weaker nonlinearity $g_0/10$ in a disorder potential with $U_0 = 0.2\epsilon$ and $\sigma = 0.32\xi$. In this case the initial wave function corresponds to the ground state of the GPE for $g_0/10$.

data also with Ref. [17]). To stay numerically on the safe side during long-time evolutions we performed also calculations with $g_0/10$. The exponent is predicted to be independent of nonlinearity [58]. Note that for a direct comparison the time in units used in this paper is to be scaled by a factor[2] of 1250 to obtain the units of Ref. [58]. We observe that the exponent a changes from 0.78 between $t = 0$ and $t = 100$ to 0.52 between $t = 100$ and $t = 300$ and becomes 0.34 between $t = 300$ and $t = 400$, in qualitative agreement with Ref. [58]. It should be noted, however, that the extraction of this exponent for the chaotic GPE is numerically much more challenging and less accurate than for discrete models. For example, the rigorous convergence test for time-reversed propagation [Eq. (11)] begins to fail for the longest propagation times displayed in Fig. 11.

Without spatial confinement of the system the density may become eventually sufficiently low such that the nonlinearity ($g|\psi|^2$) can be neglected compared to the disorder potential and the system reacts by localization in the linear regime. The experimentally observed Anderson localization of expanding BECs [7] is likely associated with the approach of the linear

regime. However, the presence of subdiffusive expansion due to residual nonlinearities cannot be ruled out.

A further interesting observation is that the variances (Δx) for the two nearby initial states ψ_1 and ψ_2 agree well (Fig. 11). Despite the intrinsic randomness of the propagated condensate wave functions on length scales of the potential, averages such as Δx agree very well with each other.

VI. DISCUSSION AND CONCLUSIONS

We have shown that the expansion of the condensate wave function described by the GPE features wave chaos as determined by a positive Lyapunov exponent in Hilbert space. We find wave chaos to be generic, that is, present for a variety of one-body potentials $U(x)$, including weak periodic, aperiodic, and random potentials. The wave functions develop on the length scale of the healing length and of the local variation of $U(x)$ fluctuations with amplitudes and phases exponentially sensitive to the initial state such that nearby states become approximately orthogonal to each other. We note a remarkable exception: For harmonic potentials, $U(x) = \frac{1}{2}x^2$, wave chaos is absent as a consequence of the harmonic potential theorem for many-body states [59].

The physical implications of these findings are of considerable interest and raise many conceptual questions. Wave chaos is a signature of the development of condensate density fluctuations. For a weakly interacting Bose gas condensate density fluctuations coincide with total density fluctuations of the many-body system and represent long-wave phonon excitations. For stronger interactions, the delayed onset of exponential divergence may delimit the characteristic time over which the GPE for the condensate is capable of describing the expanding BEC. Beyond this time, the expanding condensate is depleted by multiple excitations which the GPE attempts to mimic within a mean-field one-particle wave function by random fluctuations. Simply put, in this regime wave chaos may mark the breakdown of the mean-field approximation. Such reasoning would be based on the lack of exponential sensitivity to initial conditions in the real many-body system. If we consider two many-body wave functions for N particles, $\psi_1(x_1,\ldots,x_N,t = 0)$ and $\psi_2(x_1,\ldots,x_N,t = 0)$, expanded in the basis of energy eigenfunctions $\psi_n(x_1,\ldots,x_N)$ of the underlying Hamiltonian: $\psi_1(x_1,\ldots,x_N,t = 0) = \sum_n c_n \psi_n(x_1,\ldots,x_N)$ and $\psi_2(x_1,\ldots,x_N,t = 0) = \sum_n c'_n \psi_n(x_1,\ldots,x_N)$, the distance function $d^{(2)}(\psi_1,\psi_2)$ remains constant irrespective of the choice of the underlying Hamiltonian. The overlap of wave functions does not change in time. This fundamental property of linear time evolution should be reproduced by any approximative theory. However, the difficulty with this argument lies in the fact that the distance function $d^{(2)}$ in the many-body Hilbert space $\mathcal{H} = \prod_{i=1}^{N}(L^2)^i$ is unrelated to that in the L^2 space of the reduced mean-field wave function entering the GPE. Moreover, ensemble expectation values, such as the moments of the distribution (e.g., Δx discussed above), which represent averages over the condensate wave function over fine-scale density fluctuations, are found to be insensitive to small variations of the initial state. The GPE may remain predictive for such expectation values on longer times scales. The latter would explain the large number of successful applications of

the GPE to condensate expansions (see, e.g., Refs. [3,7–9,13]). Such a link between chaotic wave functions and observables would be analogous to classical chaos for particles and phase-space distribution functions: While the long-time evolution of individual trajectories becomes unpredictable, the ensemble or time average over stochastic regions in phase space remain well defined and yield stable ensemble expectations values. Going beyond large-scale averaging, the characterization of the fine-scale random fluctuations developing under propagation with the GPE remains a widely open problem. Propagation of many-body wave functions beyond the GPE may shed light on the question to which extent the GPE fluctuations, in the mean-field level, may faithfully represent at least some of the features of multi-particle excitation. The latter may also provide insight into the applicability of a wave function "thermalization hypothesis" originally developed for wave functions of the LSE for classically chaotic systems [60] to wave chaos in the GPE. Furthermore, it would be of interest to experimentally search for and characterize local fluctuations and structures in expanding condensates, for example, by elastic light scattering.

[1] M. Inguscio, S. Stringari, and C. E. Wieman (editors), in *Proceedings of the International School of Physics "Enrico Fermi," Course CXL, Varenna, 7–17 July* 1998 (IOS Press, Amsterdam, 1999).

[2] F. Dalfovo, S. Giorgini, L. P. Pitaevskii, and S. Stringari, Rev. Mod. Phys. **71**, 463 (1999).

[3] J. E. Lye, L. Fallani, M. Modugno, D. S. Wiersma, C. Fort, and M. Inguscio, Phys. Rev. Lett. **95**, 070401 (2005).

[4] C. Fort, L. Fallani, V. Guarrera, J. E. Lye, M. Modugno, D. S. Wiersma, and M. Inguscio, Phys. Rev. Lett. **95**, 170410 (2005).

[5] T. Schulte, S. Drenkelforth, J. Kruse, W. Ertmer, J. Arlt, K. Sacha, J. Zakrzewski, and M. Lewenstein, Phys. Rev. Lett. **95**, 170411 (2005).

[6] D. Clément, A. F. Varón, M. Hugbart, J. A. Retter, P. Bouyer, L. Sanchez-Palencia, D. M. Gangardt, G. V. Shlyapnikov, and A. Aspect, Phys. Rev. Lett. **95**, 170409 (2005).

[7] J. Billy *et al.*, Nature (London) **453**, 891 (2008).

[8] G. Roati, C. D'Errico, L. Fallani, M. Fattori, C. Fort, M. Zaccanti, G. Modugno, M. Modugno, and M. Inguscio, Nature (London) **453**, 895 (2008).

[9] D. Dries, S. E. Pollack, J. M. Hitchcock, and R. G. Hulet, Phys. Rev. A **82**, 033603 (2010).

[10] T. Dauxois and M. Peyrard, *Physics of Solitons* (Cambridge University Press, Cambridge, 2006).

[11] D. Jaksch and P. Zoller, Ann. Phys. **315**, 52 (2005).

[12] I. Bloch, J. Dalibard, and W. Zwerger, Rev. Mod. Phys. **80**, 885 (2008).

[13] Y. P. Chen, J. Hitchcock, D. Dries, M. Junker, C. Welford, and R. G. Hulet, Phys. Rev. A **77**, 033632 (2008).

[14] B. Deissler, M. Zaccanti, G. Roati, C. D'Errico, M. Fattori, M. Modugno, G. Modugno, and M. Inguscio, Nat. Phys. **6**, 354 (2010).

[15] L. Sanchez-Palencia and M. Lewenstein, Nat. Phys. **6**, 87 (2010).

[16] T. Paul, P. Leboeuf, N. Pavloff, K. Richter, and P. Schlagheck, Phys. Rev. A **72**, 063621 (2005).

[17] L. Sanchez-Palencia, D. Clément, P. Lugan, P. Bouyer, G. V. Shlyapnikov, and A. Aspect, Phys. Rev. Lett. **98**, 210401 (2007).

[18] M. Albert, T. Paul, N. Pavloff, and P. Leboeuf, Phys. Rev. Lett. **100**, 250405 (2008).

[19] S. E. Skipetrov, A. Minguzzi, B. A. van Tiggelen, and B. Shapiro, Phys. Rev. Lett. **100**, 165301 (2008).

[20] S. Flach, D. O. Krimer, and C. Skokos, Phys. Rev. Lett. **102**, 024101 (2009).

[21] T. Ernst, T. Paul, and P. Schlagheck, Phys. Rev. A **81**, 013631 (2010).

[22] B. Wu and Q. Niu, Phys. Rev. A **64**, 061603(R) (2001).

[23] B. Wu and Q. Niu, New. J. Phys **5**, 104 (2003).

[24] V. V. Konotop and M. Salerno, Phys. Rev. A **65**, 021602(R) (2002).

[25] M. Machholm, C. J. Pethick, and H. Smith, Phys. Rev. A **67**, 053613 (2003).

[26] O. Morsch and M. Oberthaler, Rev. Mod. Phys. **78**, 179 (2006).

[27] E. Fermi, J. R. Pasta, and S. Ulam, Los Alamos Scientific Laboratory Report No. LA-1940, 1955.

[28] T. Dauxois, Phys. Today **61**, 55 (2008).

[29] B. M. Herbst and M. J. Ablowitz, Phys. Rev. Lett. **62**, 2065 (1989).

[30] P. Villain and M. Lewenstein, Phys. Rev. A **62**, 043601 (2000).

[31] A. C. Cassidy, D. Mason, V. Dunjko, and M. Olshanii, Phys. Rev. Lett. **102**, 025302 (2009).

[32] M. J. Ablowitz, C. Schober, and B. M. Herbst, Phys. Rev. Lett. **71**, 2683 (1993).

[33] Y. Lahini, A. Avidan, F. Pozzi, M. Sorel, R. Morandotti, D. N. Christodoulides, and Y. Silberberg, Phys. Rev. Lett. **100**, 013906 (2008).

[34] T. N. Rescigno and C. W. McCurdy, Phys. Rev. A **62**, 032706 (2000).

[35] C. W. McCurdy, D. A. Horner, and T. N. Rescigno, Phys. Rev. A **63**, 022711 (2001).

[36] B. I. Schneider and L. A. Collins, J. Non-Cryst. Solids **351**, 1551 (2005).

[37] B. I. Schneider, L. A. Collins, and S. X. Hu, Phys. Rev. E **73**, 036708 (2006).

[38] A. Askar and A. S. Cakmak, J. Chem. Phys. **68**, 2794 (1978).

[39] C. Leforestier *et al.*, J. Comput. Phys. **94**, 59 (1991).

[40] G. Engeln-Müllges and F. Uhlig, *Numerical Algorithms with Fortran* (Springer-Verlag, Berlin Heidelberg, 1996).

[41] H. De Raedt, Comp. Phys. Rep. **7**, 1 (1987).

[42] J. Laskar and P. Robutel, Celestial Mech. Dyn. Astron. **80**, 39 (2001).

[43] T. J. Park and J. C. Light, J. Chem. Phys. **85**, 5870 (1986).

[44] M. Ablowitz, B. M. Herbst, and C. M. Schober, J. Comput. Phys. **131**, 354 (1997).

[45] D. J. Kouri, D. S. Zhang, G. W. Wei, T. Konshak, and D. K. Hoffman, Phys. Rev. E **59**, 1274 (1999).

[46] W. Eckhaus and A. van Harten, *The Inverse Scattering Transform and the Theory of Solitons* (North-Holland, Amsterdam, 1981).

[47] M. J. Ablowitz and P. A. Clarkson, *Solitons, Nonlinear Evolution Equations and Inverse Scattering* (Cambridge University Press, Cambridge, 1991).

[48] P. G. Drazin and R. S. Johnson, *Solitons: An Introduction* (Cambridge University Press, Cambridge, 1996).

[49] Z. X. Liang, Z. D. Zhang, and W. M. Liu, Phys. Rev. Lett. **94**, 050402 (2005).

[50] R. Atre, P. K. Panigrahi, and G. S. Agarwal, Phys. Rev. E **73**, 056611 (2006).

[51] V. N. Serkin, A. Hasegawa, and T. L. Belyaeva, Phys. Rev. Lett. **98**, 074102 (2007).

[52] H. H. Chen and C. S. Liu, Phys. Rev. Lett. **37**, 693 (1976).

[53] U. Al Khawaja, Phys. Rev. E **75**, 066607 (2007).

[54] X. G. He, D. Zhao, L. Li, and H. G. Luo, Phys. Rev. E **79**, 056610 (2009).

[55] U. A. Khawaja, J. Math. Phys. **51**, 053506 (2010).

[56] S. B. Kuksin, *Nearly Integrable Infinite-Dimensional Hamiltonian Systems* (Springer-Verlag Berlin Heidelberg, 1993).

[57] A. S. Pikovsky and D. L. Shepelyansky, Phys. Rev. Lett. **100**, 094101 (2008).

[58] T. V. Laptyeva, J. D. Bodyfelt, D. O. Krimer, C. Skokos, and S. Flach, Eur. Phys. Lett. **91**, 30001 (2010).

[59] J. F. Dobson, Phys. Rev. Lett. **73**, 2244 (1994).

[60] M. Srednicki, Phys. Rev. E **50**, 888 (1994).